Available online at www.sciencedirect.com

ScienceDirect

Energy Procedia 63 (2014) 5394 – 5407

Energy Procedia

GHGT-12

Impacts of Injection Induced Fractures Propagation in CO_2 Geological Sequestration – Is Fracturing Good or Bad for CO_2 Sequestration

Zhiyuan Luo[a,b], Steven Bryant[a,c]*

[a] *Department of Petroleum and Geosystems Engineering, The University of Texas at Austin, Austin, TX 78712, USA*
[b] *Current address:Degolyer and MacNaughton Inc., Dallas, TX 75244, USA*
[c] *Current address: Department of Chemical and Petroleum Engineering, University of Calgary, Calgary, AB, T2N 1N4, Canada*

Abstract

In large-scale CO_2 sequestration project the formation temperature decreases as huge amounts of relatively cool CO_2 are injected. Injection induced fractures from injectors are facilitated as the critical pressure in the formation for fracturing is reduced by considerable thermo-elastic stress, which is proportional to the temperature difference between CO_2 and reservoir . In this study, we analyze injection induced fracture growth and its impact on CO_2 plume migration by a semi-analytical quasi-steady state model in the case that injection induced fractures are permitted by regulators. By parametric analysis with the model, geological properties and operating conditions are investigated to show their sensitivity on fracture growth and CO_2 migration. This work provides analytical tools, which enable fast and simple screening of appropriate storage sites and of injection strategy, to predict fracturing and CO_2 migration to avoid potential risks.

Peer-review under responsibility of the Organizing Committee of GHGT-12

Keywords: CO_2 sequestration; thermal induced fracturing; two-phase flow model

1. Introduction

In large-scale geological CO_2 sequestration, high injection rate is required to satisfy economics and operational considerations. Due to huge amount of cool CO_2 injected, the formation temperature reduces substantially and this

* Corresponding author. Tel.: +1-403-220-6554
E-mail address: steven.bryant@ ucalgary.ca

Peer-review under responsibility of the Organizing Committee of GHGT-12
doi:10.1016/j.egypro.2014.11.570

may re-distribute the in-situ stresses and lower the critical pressure for fracture initiation and propagation. Since fractures have potential risk for leakage, they may not be permitted by rigorous regulators [1]. However, in the more flexible case that regulators allow suitably contained fractures, e.g. within a certain area of review within the storage reservoir, not propagating above the storage formation, etc., more formations would be available for CO_2 storage. An important motivation for allowing fracture propagation within the storage formation is that it greatly enhances injectivity. On the other hand, such fractures also influence the CO_2 migration pattern. Slow growth fracture can increase injectivity without changing flood region shape (Fig. 1b); while fast propagation increases injectivity but stretches flood region very flat in fracture growing direction and thus results in CO_2 arriving drainage area boundary in a shorter time (Fig. 1a). Therefore, predictions and monitoring on fracture growth and their impact on CO_2 plume migration are very important to site screening and risk control.

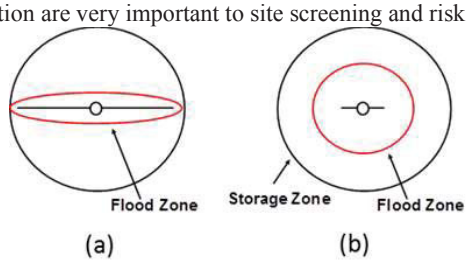

Figure 1. Sketch of injection induced fractures with different length and their corresponding geometry of CO_2 migration areas: (a) fast growth long fracture; (b) slow growth short fracture.

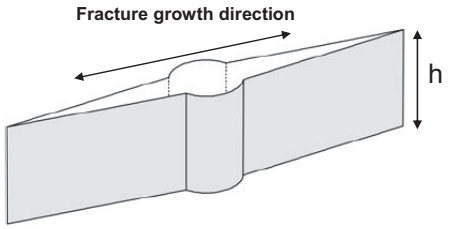

Figure 2. Sketch of injection induced vertical fracture from perforated portion of vertical injector.

In this work, a semi-analytical quasi-steady state model of coupled fracture growth and CO_2 plume migration has been built. The mechanism of fracture growth of interest in this work is mainly based on the impact of thermally induced stress. Due to the reduction in minimum horizontal stress by the thermoelastic stress, the critical pressure for fracture growth at fracture tip can be much lower than the pressure required for hydraulic fracturing treatment. The magnitude of the reduction depends on the injection rate and formation conditions [1]. If injection induced fracture occurs, flooding system will evolve from a circular geometry in the map view to an ellipse, where the oblateness of flood area depends on fracture length and how fast the fracture grows.

The model is extended from Perkins and Gonzalez's model [2], which was originally developed for water flooding in oil reservoir, to account for propagation of fractures from CO_2 injection wells in brine-filled formations. The fracture propagation criterion is based on fracture mechanics by introducing the concept of rock fracture toughness and taking account of poro-elastic and thermo-elastic stresses. The evolving elliptical shape of the flood front and thermal front are determined from fracture length and injection rate. By extending Buckley-Leverett theory in elliptic coordinate system, we introduce a two-phase fractional flow model for vertical fractured well [3]. Combining this model with fracture propagation model, we can more accurately predict evolution of CO_2 and brine migration in storage formation. Finally, based on qualitative analysis, conclusions are given about fractures propagation and CO_2 flow migration.

2. Modeling Approach

2.1. Single-phase flow injection induced fracture growth model

In this model, injection induced fracture from vertical injector is simplified as a two-wing like shape (Fig. 2). In CO_2 sequestration process, storage formation is cooled down and in-situ minimum horizontal stress decreases due to thermo-elastic effect. Stresses in upper and lower impermeable sealing layers do not change. The increased difference between in-situ minimum horizontal stress in storage formation and that in sealing formation makes it unlikely that the injection induced fracture can propagate into the overburden or underburden formation. Therefore, the cooling effect improves fracture height containment. In the map view of CO_2 injection from fractured vertical well in Fig. 3, we see a region with cooled formation (inside blue ellipse) and cool CO_2; this region is sharply

separated from regions at original reservoir temperature by the interface defined as thermal front (blue ellipse). Similarly, the interface between brine and CO_2 is defined as flood front (red ellipse). Between the two fronts, the fluid is injected CO_2 warmed to reservoir temperature by formation rock and residual brine. Fracture mechanics studies dictate that the face of fracture is perpendicular to the direction of minimum principal stress, which is minimum horizontal stress in normal faulting stress regime formations.

The procedure of our semi-analytical quasi-steady state model to estimate fracture growth and CO_2-brine migration is shown in Fig. 4. In section 2.1, we introduce the model with single phase piston-like fluid displacing process in an open boundary system, assuming CO_2 not dissolvable in brine. There are several aspects of this model that can be considered separately as the following.

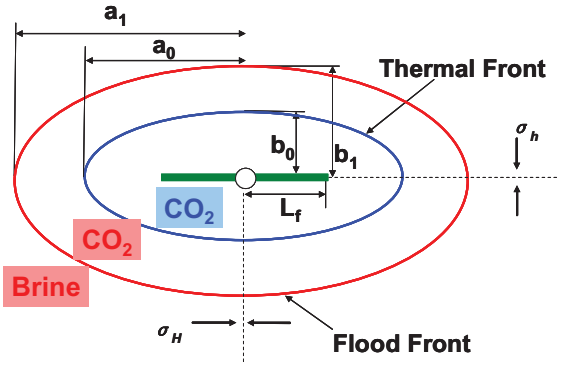

Figure 3. Map view showing a two-winged infinite conductivity vertical fracture (dark green line) of half length L_f oriented perpendicular to the plane of minimum horizontal stress (σ_h). The two ellipses stand for thermal front (blue) and flood front (red) during CO_2 injection process, respectively. Fluids in CO_2 storage aquifer occupy three regions divided by the two fronts: a cool CO_2 zone between the fracture and the thermal front, warm CO_2 zone between thermal front and flood front, and warm brine zone beyond flood front.

2.1.1. Fracture initiation criterion

Here we briefly introduce fracture initiation criterion used in the model as shown in Fig. 4. Since most formations are not perfectly intact and may contain pre-existing faults, veins, and fractures, we assume the storage formation has pre-existing flaws around injection well. Therefore, fracture has already initiated and it would grow once fracture propagation condition satisfied. We assume an initial fracture length (L_{f0}) equal to at least twice the wellbore radius as in previous literature [4]. The fracture initiation pressure for formations with flaws is

$$P_{frac}^{T} = \sigma_h + \Delta\sigma^{T}(L_{f0}) + \Delta\sigma^{P}(L_{f0}) + \frac{K_{IC}}{\sqrt{\pi L_{f0}}} \qquad (1)$$

where σ_h is minimum horizontal stress, $\Delta\sigma^T$ is thermo-elastic stress, $\Delta\sigma^P$ is poro-elastic stress, and K_{IC} is Mode-I rock fracture toughness (tensile open fracture).

2.1.2. Fracture propagation criterion

If pressure at fracture tip (P_{tip}) is higher than Eq. (1), fractures would grow. Eq. (2) is the criterion for continued fracture propagation after initiation

$$P_{tip} \geq P_{frac}^{prop} \qquad (2)$$

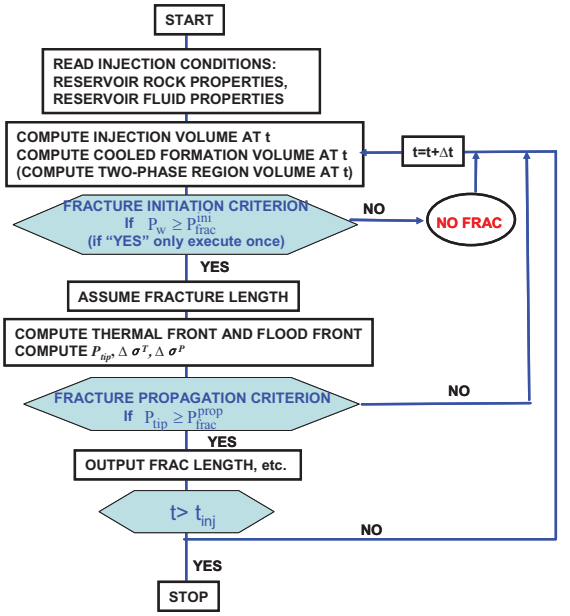

Figure 4. Flow chart of fracture growth modeling

The pressure for fracture propagation in Eq. (2) contains two parts as shown in Eq. (3): (I) Pressure required to keep fracture open towards local minimum horizontal stress; (II) Pressure required to overcome resistance at fracture tip and create new fracture volume. In part (I), original horizontal minimum stress is reduced

by thermo-elastic stress ($\Delta\sigma^T$, quantity is negative due to cooling) and increased by poro-elastic stress ($\Delta\sigma^P$, quantity is positive due to pressure increase by injection

$$P_{frac}^{prop} = \underbrace{\sigma_h + \Delta\sigma^T(L_f) + \Delta\sigma^P(L_f)}_{\text{(I)}} + \underbrace{\frac{K_{IC}}{\sqrt{\pi L_f}}}_{\text{(II)}} \tag{3}$$

where $\Delta\sigma^T$ and $\Delta\sigma^P$ is variable with geometry of thermal front, L_f is fracture half length.

$$\Delta\sigma^T = \frac{\alpha_T E \Delta T}{(1-\nu)} \bullet f(a_0, b_0, h) \tag{4}$$

$$\Delta\sigma^P = \alpha_p \Delta P \bullet f(a_0, b_0, h) \tag{5}$$

in which α_T is thermoelasticity coefficient, E is Young's modulus, ν is Poisson's ratio, poroelasticity coefficient is defined as $\alpha_p = Biot \cdot \frac{1-2\nu}{1-\nu}$, ΔT is formation temperature change at fracture tip due to CO_2 injection, ΔP is formation pressure change at fracture tip due to CO_2 injection, h is formation thickness, a_0 and b_0 are defined as in Fig. 3, and the function f accounts for geometric effects [2]. As noted, ΔT is negative and not a constant but calculated by heat transfer model of vertical injector in our previous work [5].

2.1.3. Pressure at fracture tip

By assuming constant pressure at open boundary, the pressure at fracture tip in Eq. (2) is the sum of series of pressure drop from drainage boundary to fracture tip as shown in Fig. 5.

$$P_w = P_{tip} = P_{bc} + \Delta P = P_R + \Delta P_1 + \Delta P_2 + \Delta P_3 \tag{6}$$

where P_R is initial formation pressure. Because of open boundary assumption, P_{bc} keeps its initial value P_R. Bottom hole pressure is equal to pressure at fracture tip if fracture has infinite conductivity. The calculations of ΔP_1, ΔP_2 and ΔP_3 could be seen in [3].

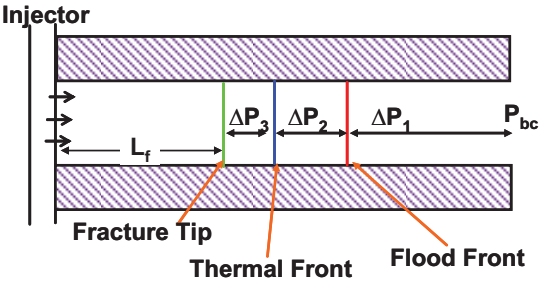

Figure 5. Side view of one wing of injection induced fractures and sketch of pressure drops in each zone (ref. Fig. 3). P_{bc} is pressure at drainage area boundary.

2.1.4. CO_2-brine fluid migration

Since $\Delta\sigma^T$ and $\Delta\sigma^P$ in Eq. (4) and Eq. (5) are functions of geometry of thermal front, the calculation of cooled area inside thermal front is based on energy balance [2]. Ignoring heat transferred from overburden and underburden formations and heat transfer between cool and warm regions, we determine cool and warm region by conserving enthalpy as,

$$V_T = \frac{\rho_{co_2} C_{co_2} Q(t)}{\rho_{gr} C_{gr}(1-\phi) + \rho_{co_2} C_{co_2} \phi \cdot 1} \tag{7}$$

where C_{co2} is specific heat capacity of CO_2 in subsurface state, C_{gr} is specific heat capacity of formation rock grains, ρ_{co2} is the density of CO_2 in storage formation, ρ_{gr} is the density of formation rock grains. Similarly, the volume of CO_2 flooded region is calculated by material balance as

$$V_{inj} = \frac{Q}{\phi(1 - S_{wr})} \tag{8}$$

where ϕ is formation porosity, S_{wr} is residual brine saturation in CO_2 flooded region, Q is total injected volume.

Injected CO_2 migrates from a fractured vertical well with an elliptical shape front. The fronts of the CO_2 flooded regions and regions with different temperature are confocal with fracture, as in Fig. 3. The procedure with more details for calculations of axes of these ellipses was discussed in [3].

By running the model as the third box in flow chart as shown in Fig. 4, we can simply estimate fracture growth and CO_2 migration from a fractured vertical injector.

2.2. Two-phase flow injection induced fracture growth model

Since brine can dissolve into supercritical state CO_2 and vice versa, the single phase model is not accurate to illustrate fluid migration in CO_2-brine system. Although numerical simulations provide detailed information about mixture zone with two phases (CO_2-saturated water and water-saturated CO_2), it takes much cost and time. To simply describe boundaries (dry front and flood front) and saturations ($S_{g,dry}$ and $S_{g,BL}$) of two-phase zone, as shown in Fig. 6, Buckley-Leverett fractional flow theory is extended to apply for fractured vertical injector.

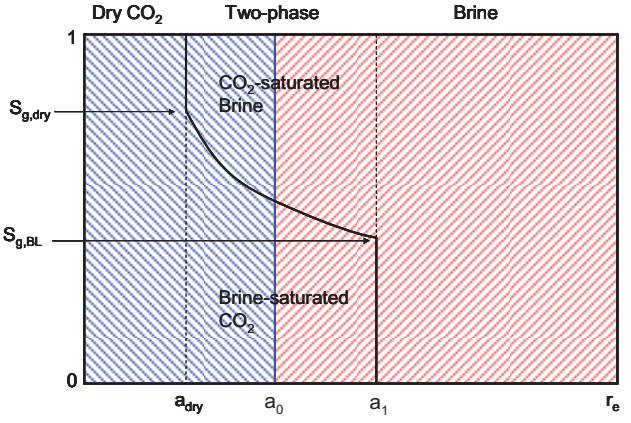

Figure 6. Four regions of CO_2 migration during injection with two-phase flow model. Besides pure CO_2 and brine zones, a two-phase zone of CO_2-brine mixture is designed with Buckley-Leverett Theory in elliptic coordinate system. The thermal front divides the entire formation to two parts, cooled zone (under blue shade) and warm zone (under red shade). The fractional flow curve modified to account for multiphase transport of CO_2-brine determines the positions of dry front (a_{dry}) and flood front (a_1) and the saturations in the two-phase Buckley-Leverett region.

Traditional Buckley-Leverett theory is valid for 1-dimension immiscible displacement from vertical injector. Similar to the approaches in previous literature [6,7] which applied the fractional flow theory in radial flow from unfractured injectors, here we will build elliptic coordinate system and determine speed of fronts and phase saturation on each side of fronts by using the extended fractional flow theory as the following. Values of all properties used for extending fractional flow calculation in [3] are listed in Table 1.

The cooled volume depends on the position of thermal front. As shown in Fig. 7, thermal front may locate at two possible positions, either in dry CO_2 region or in two-phase region, depending on total heat capacity of formation rocks. We conceptually determine the cool and warm regions from energy balance as in single-phase flowing CO_2-displacing-brine model. The details of identification of each region in Fig. 7 and its pressure drop can be seen in [3]. The total pressure drop from wellbore to storage reservoir boundary is

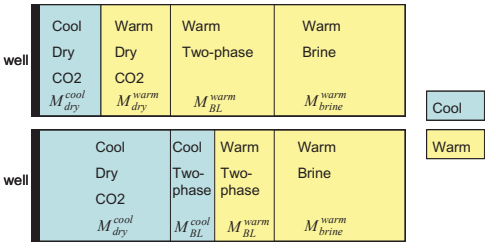

Figure 7. Two possible patterns of CO_2-brine displacement flow regions: (above) cool region (light blue) smaller than dry CO_2 region (light brown), as $V_T < V_{dry}$; (below) cool region larger than dry CO_2 region, as $V_T > V_{dry}$.

(a) $V_T < V_{dry}$

$$\Delta P = \Delta P_{dry}^{cool} + \Delta P_{dry}^{warm} + \Delta P_{BL}^{warm} + \Delta P_{brine}^{warm} \quad (9)$$

(b) $V_T > V_{dry}$

$$\Delta P = \Delta P_{dry}^{cool} + \Delta P_{BL}^{cool} + \Delta P_{BL}^{warm} + \Delta P_{brine}^{warm} \quad (10)$$

From the above equations, we have

$$P_{tip} = P_R + \Delta P \quad (11)$$

By adding the information of two-phase region during CO_2-brine migration, bottom hole pressure could be more accurately estimated and thus fracture growth. The rest of the procedure for fracture growth calculation is the same as that in single phase flow model (Section 2.1) and thus we do not repeat it here.

Table 1 - Sandstone Properties

$D_{brine \to BL}$	-0.0582
$D_{BL \to dry}$	1.0469
S_{wr}	0.4230
$k_{rg}^{\ o}$	0.2638
m	1.7
n	2.8

3. Results and Discussions

3.1. A study example

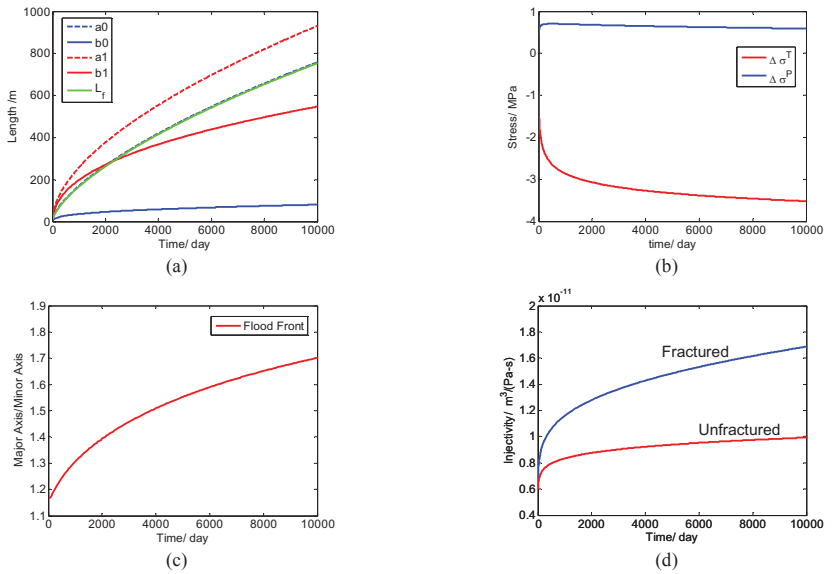

Figure 8. Analysis of a case of CO_2 injection induced fracture growth: (a) fracture growth and fronts growth: green line stands for fracture length versus time, red dash line and solid line are major axis and minor axis of flood front, blue dash line and solid line are major axis and minor axis of thermal front; (b) thermo-elastic stress (red) and poro-elastic stress (blue) at fracture tip versus time; (c) the ratio of major axis over minor axis of flood front versus time; (d) injectivity versus time of fractured and unfractured vertical injectors. Values of all parameters used here are given in Table 2

Before sensitivity study on related parameters, we first introduce a case study by the models and approaches described in the last section. The values of parameters used in this case are listed in Table 2 unless specified. In Fig. 8(a), it shows fracture grows faster at early time and propagation speed declines with time. In this case, we see fracture tip (green curve) is at the same position as thermal front tip (blue dash curve). Fracture tip cannot pass thermal front since pressure for fracturing in the region beyond the thermal front is much higher than the cooled region inside thermal front, because there is no reduction due to thermo-elastic stress outside. From Fig. 8(b), we can see the reason that pressure require for fracture propagation declines with time is because the magnitude of the thermo-elastic stress increases with time. Moreover, thermo-elastic stress is dominant compared to poro-elastic stress during injection process. In Fig. 8(c), we note that the ratio of major axis over minor axis of the flood front (a_1/b_1) increases with time, which means the ellipse of CO_2-brine boundary is growing flatter by fracture growth. Along with fracture growth, flooding pattern physically leaves plenty area unswept in the direction perpendicular to fracture. In other words, fractures shorten the breakthrough time of CO_2 flood front to storage formation boundary. As bottom hole pressure of fractured injector is much lower than unfractured injector at the same injection rate, the injectivity increases with time due to the incremental conductivity provided by new growth fracture (in Fig. 8(d)). For the case of unfractured injector shown here, it is a virtual scenario presented only for illustration; in practice the bottom hole pressure would exceed fracture criterion pressure and the wellbore would fracture under these conditions.

In the same formation, we investigate the impact of injection rate on fracture growth as shown in Fig. 9. We observe the length of fracture (green curve) and the distance of CO_2 flood front in major direction (red curve) from injector after 10,000 days injection. Above threshold injection rate (1530 m^3/d), fracture length is non-linear to injection rate in a narrow interval and then grows linearly with injection rate. The tip of flood front increases linearly before threshold injection rate of fracture growth. After threshold injection rate, its relation turns from non-linear to linear with injection rate. It is important to notice, at high injection rate, fracture tip reaches flood front as the two curves overlap each other. This implies that the injection induced fracture reaches storage system boundary once flood front breakthrough drainage area, where CO_2 may easily leak out and contaminate surrounding environment.

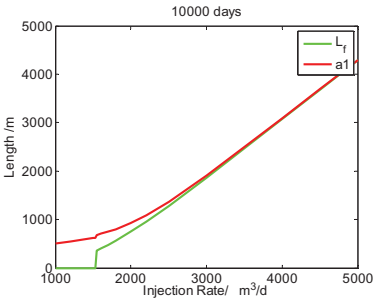

Figure 9. Fracture growth and major axis of flood front growth versus injection rate.

3.2. Parametric analysis on geological factors

To comprehensively understand factors on fracture growth and CO_2 migration, parametric analysis on geological parameters are conducted and the results are discussed as the following.

3.2.1. Young's Modulus (E)

Young's modulus is a major factor on thermo-elastic stress which is the reason that critical pressure for fracture growth reduces at fracture tip. As shown in Fig. 10(a) of formation with low Young's modulus (10 GPa), fracture stops after 3910 days propagation to 86.2m. In this special case, from the fourth panel of Fig. 10(a), we can see bottom hole pressure declines faster than fracture propagation pressure. At fixed injection rate, only when Young's modulus is in low value, fracture growth is "grow and stop" mode. Compared to drainage radius (10000m), approximately, we can ignore the influence of this short fracture on CO_2 migration, as flooded area is almost in circle shape with a_1/b_1 equal to 1.009 (a_1 is about 716m) after 10000 days injection (the second panel). However, the injectivity indeed acquires benefit from fracture, increasing to 1.43 times of unfractured injector. Therefore, short fractures during injection are generally favorable.

In Fig. 10(b), formation with medium Young's modulus (12 GPa), fracture grows as fast as thermal front (753 m after 10000 days injection), which stretches the region flooded (931 m after 10000 days injection) by CO_2 into an elliptical geometry. Flood front in major axis moves faster than the case in Fig. 10(a). With Young's modulus increasing to 14GPa, as shown in Fig. 10(c), fracture grows almost as fast as flood front in major direction (L_f = 1336 m and a_1 = 1386 m) and the flooding ellipse is much flatter than those of the preview two cases. In this case, as fracture tip almost reaches flood front, cool CO_2 flows from wellbore and along fracture and thereby directly reaches flood front. Thermal front thus overlaps with flood front in fracture growing direction. In contrast to ideal flood pattern as a circle shape, this flatter ellipse area is the consequence of fast fracture growth in major axis direction. The geometry leads to a quick arrival of CO_2 at formation boundaries and low usage efficiency of storage site. Comparing all cases, we can conclude that the higher Young's modulus, the faster fracture growth, the quicker flood front breakthrough, and the lower usage efficiency of storage site. The case of fracture stopping only exists in formations with low Young's modulus.

Table 2 - Base case values for CO_2 injection induced fracture analysis

Injection operation properties	
Formation depth, D	1000 m
Formation thickness, h	50 m
Injection rate, q	2000 m^3/d
Injection period	10000 days
Wellhead CO_2 temperature, $T(0)$	15 °C
Earth surface temperature, $T_{fm}(0)$	20 °C
Wellbore radius, r_w	0.1 m
Storage formation radius, r_e	10,000 m
Formation rock properties	
Compressibility of rock grain, c_{gr}	2.2×10^{-11} Pa^{-1}
Compressibility of formation, c_f	4.8×10^{-10} Pa^{-1}
Young's modulus, E	12 GPa
Poisson's ratio, v	0.35
Thermoelasticity coefficient, α_T	1.0×10^{-5} K^{-1}
Geothermal gradient, G	30 °C/km
Formation permeability, k	100 md
Formation porosity, ϕ	0.25
Endpoint relative permeability CO_2 phase, k_{rg}	0.8
Unit volume rock grain heat capacity, $\rho_{gr}C_{gr}$	2340 kJ/(m^3-K)
Formation fluid properties	
Formation fluid density, ρ_w	1000 kg/m^3
Mean density of supercritical CO_2, ρ_{co2}	800 kg/m^3
Compressibility of brine at subsurface condition, c_w	5.2×10^{-10} Pa^{-1}
Compressibility of CO_2 at subsurface condition, c_g	1.66×10^{-8} Pa^{-1}
Volumetric Specific heat capacity of brine, C_w	4200 kJ/(m^3-K)
Volumetric specific heat capacity of CO_2, C_{co2}	1200 kJ/(m^3-K)
Viscosity of warm brine in the formation, $\mu_{w,warm}$	4.3×10^{-4} Pa-s
Viscosity of cool brine in the formation, $\mu_{w,cool}$	7.0×10^{-4} Pa-s
Viscosity of warm CO_2 in the formation, $\mu_{g,warm}$	4.6×10^{-5} Pa-s
Viscosity of cool CO_2 in the formation, $\mu_{g,cool}$	8.0×10^{-5} Pa-s

3.2.2. Poisson's ratio (v)

The impact of Poisson's ratio is on both thermo-elastic stress and poro-elastic stress as in Eq. (4) and Eq. (5). Reducing Poisson's ratio results in the slower growth of the fracture (in Fig. 11(a)), as the increment of thermo-elastic stress is less than the increment of poro-elastic stress (Fig. 11(b)). Due to the opposite signs of the two induced stresses, combining the two stresses increases pressure for fracture propagation. Especially, in early time, the increment of poro-elastic stress is much larger than thermo-elastic, as emphasized by grey circles in Fig. 11(b). In sum, effect of Poisson's ratio is stronger on poro-elastic stress than thermo-elastic stress.

3.2.3. Formation pore pressure (P_R)

As shown in Fig. 12(a), in formation with overpressure (1MPa), fracture grows with the speed over 2.5 times as that in normal hydrostatic formation. At the same injection rate, in formation with high pore pressure, higher bottom hole pressure is required, and high bottom hole pressure (Fig. 12(b)) is the reason of fast fracture growth. Moreover, high bottom hole pressure needs more energy for pumping.

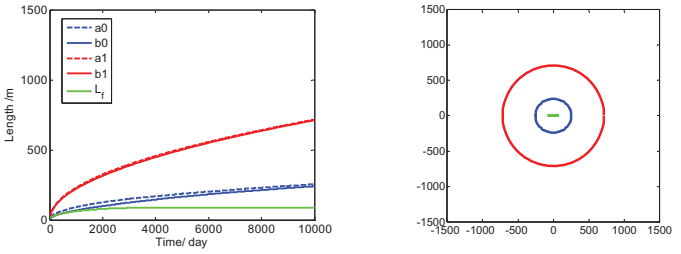

(a) E=10 GPa

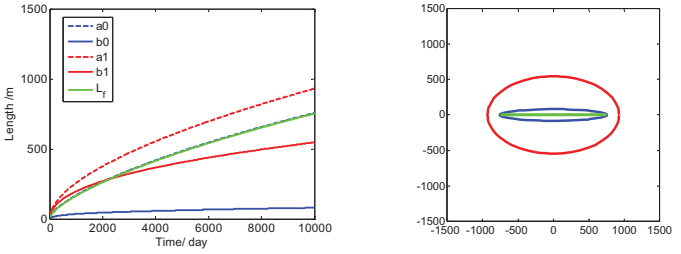

(b) E=12 GPa

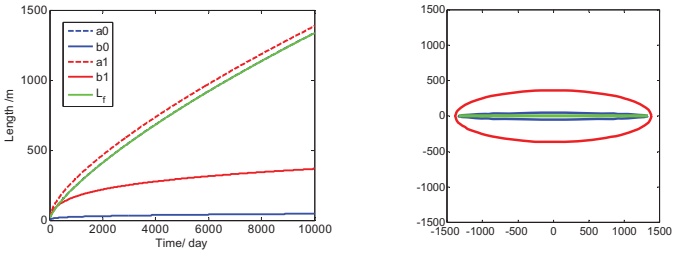

(c) E=14 GPa

Figure 10. The effect of Young's modulus of storage formation on fracture growth and shapes of flooded and cooled regions: (a) E=10 GPa; (b) E=12 GPa; (c) E=14 GPa. The left column shows fracture, thermal front, and flood front growth versus time; while the right column shows flooded and cooled regions evolution after 10,000 days CO_2 injection.

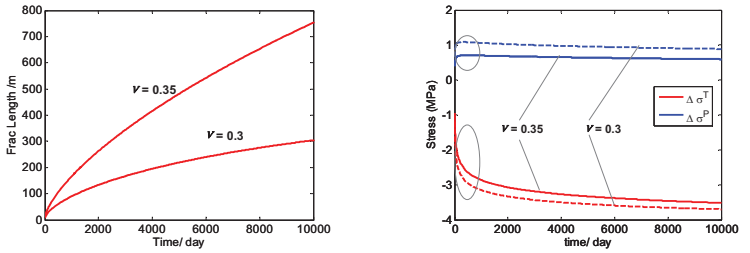

Figure 11. (a) The effect of Poisson's ratio on fracture growth; (b) Thermo-elastic stress and poro-elastic stress at ν=0.3 and 0.35. The grey circle emphasize increment of poro-elastic stress is much larger than that of thermo-elastic stress at early period of injection.

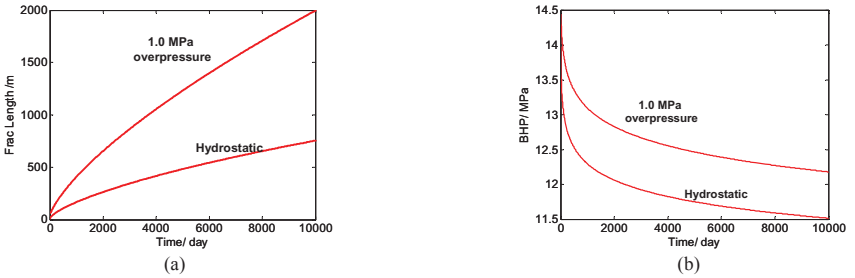

Figure 12. (a) The effect of formation pore pressure on fracture growth. Pore fluid density is ρ_f=1000 kg/m^3 in hydrostatic circumstance; while it is ρ_f=1100 kg/m^3 for 1 MPa overpressure formation; (b) bottom hole pressures of hydrostatic and overpressure formations

3.2.4. Formation porosity (ϕ)

Fracture grows faster in high porosity formation as shown in Fig. 13. With porosity increasing from 0.15 to 0.25 (66.7% increment), increment of fracture length is from 623 m to753 m (20.9% increment) and flood front is from 1030 m to 930 m (10.8% decrement) after 10000 days injection. In other words, the impact of porosity on fracture growth and fluid migration is weak. Porosity is related to two physical properties affecting the fracture propagation model: the volume for CO_2 storage and total heat capacity of rock grains.

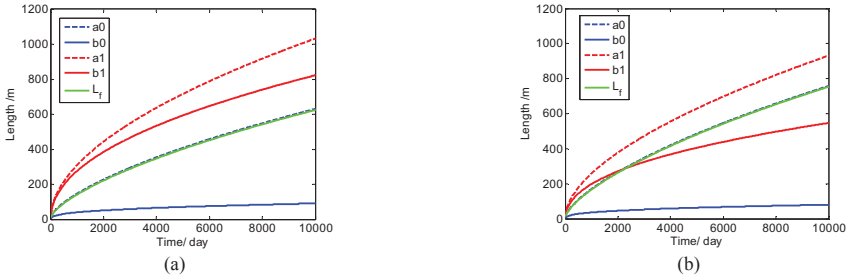

Figure 13. The effect of porosity on cooled region volume: (a) ϕ =0.15; (b) ϕ =0.25. Porosity is relevant to total heat capacity of rock grains and thus the volume of cooled region. Low porosity means more grains, which stores higher heat than that in high porosity formation, and thus results in smaller cooled region volume.

With the same amount of CO_2 injected in case (a) and (b), formation with low porosity as in Fig 13(a) takes more volume to contain CO_2 and flood front evolves farther from injector although fracture is shorter. Additionally, we notice flood region in (a) is more round (a_1/b_1 equals 1.26) than in Fig. 13(b) (a_1/b_1 equals 1.74), which means storage site usage efficiency in low porosity formation is higher.

3.2.5. Volumetric rock heat capacity ($\rho_{gr}C_{gr}$)

Volumetric rock heat capacity is another factor directly determining thermal front growth speed. The typical range of $\rho_{gr}C_{gr}$ is between 1120 kJ/(m^3-K) and 2440 kJ/(m^3-K). Here we compare two injection scenarios, with $\rho_{gr}C_{gr}$ equal to 1270 kJ/(m^3-K) and 2340 kJ/(m^3-K) in Fig. 14. As we analyzed for high porosity case, low $\rho_{gr}C_{gr}$ results low total heat capacity of rock grains and thus it needs more volume for heat transfer with injected cool CO_2. The thermal fronts move with almost the same speed in minor direction, but much faster in major direction in formations with low $\rho_{gr}C_{gr}$. As noted fracture propagates at the same speed with thermal front, fracture is longer in low $\rho_{gr}C_{gr}$ formation, which stretches flood front flatter. Under this analysis, it is not hard to conclude that fracture in formations with lower $\rho_{gr}C_{gr}$ is longer and it takes shorter time for flood front to breakthrough storage formation.

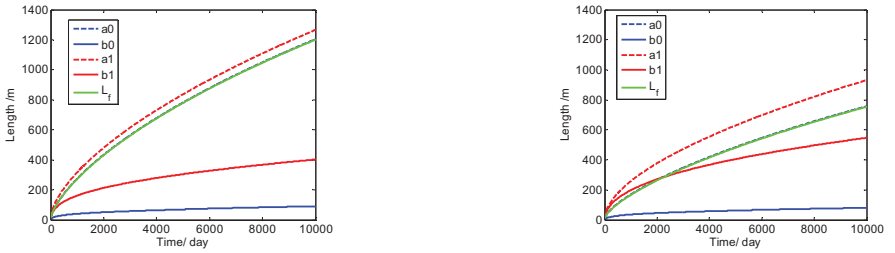

Figure 14. The effect of rock unit volume heat capacity on fracture growth: (a) $\rho_{gr}C_{gr}$=1170 kJ/(m^3-K); (b) $\rho_{gr}C_{gr}$=2340 kJ/(m^3-K).

3.2.6. *Formation permeability (k) and formation thickness (h)*

As shown in Fig. 15(a), to ensure fracturing in 100md formation, we increase injection rate to 3500 m^3/d. A high permeability formation (100 md) enable injected CO_2 to leak off through short fracture (1081 m); while low permeability formation (50 md) requires long fracture (2461 m) to provide enough conductivity. Both formations have thickness 50 m as in Table 2.

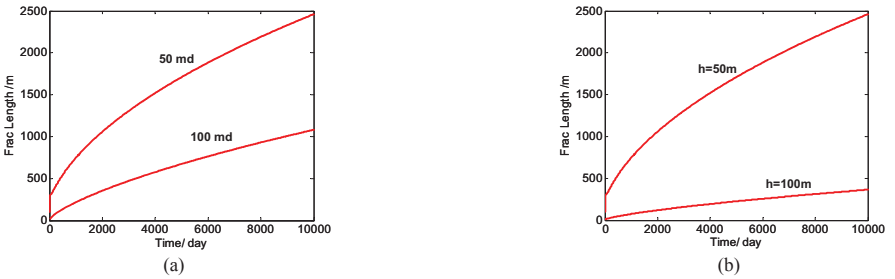

Figure 15. (a) The effect of formation permeability on fracture growth; (b) the effect of formation thickness on fracture growth

Although formation thickness (h) plays exactly the same role as formation permeability (k) on bottom hole pressure, formation thickness also determines thermo-elastic stress and poro-elastic stress in the geometry term as Eq. (4) and Eq. (5), which have considerable impact on pressure for fracture propagation as Eq. (3). As a result, critical pressure for fracture propagation is higher and bottomhole pressure is lower in thicker formations. Therefore, fracture is shorter in thicker formations, as shown in Fig. 15(b). For 50 m thickness formation, fracture length is 2461 m after 10000 day injection; while for 100 m thickness formation, fracture length is 365 m. Both formations have permeability 50 md as in Table 2. As mentioned above, the effect of formation thickness enters in geometry factor of thermo-elastic stress, and poro-elastic stress at fracture tip makes fracture length shorter (L_f=365 m) in (100 m, 50 md) formation than that (L_f=1081 m) in (50 m, 100 md) formation, although conductivities of the two formations are the same.

3.2.7. *Storage formation size (r_e)*

Size of storage site strongly affects bottomhole pressure of CO_2 injectors. In steady-state flow model, pressure drop is logarithmic to drainage area radius. Hence, bottomhole pressure monotonically increases with injection rate. As shown in Fig. 16(b), bottom hole pressure of smaller size storage formation (with drainage radius 5 km) becomes lower and lower than that in 10 km radius storage formation. In storage site with 5 km radius fracture length is 474 m after 10000 days injection while in 10 km radius formation fracture length is 85 0m (Fig. 16(a)). Correspondingly, flood front in major direction (a_1) is 796.1 m and 930.8 m. Considering formations size, flood front will break through earlier in the smaller storage site. On the other hand, comparing the shape of flooding area, it is more round

in smaller site with a_1/b_1 equal to 1.24 for site with 5 km radius and 1.71 for site with 10km radius (in Fig. 17). We can simply conclude that in small site storage usage efficiency is higher than in large site.

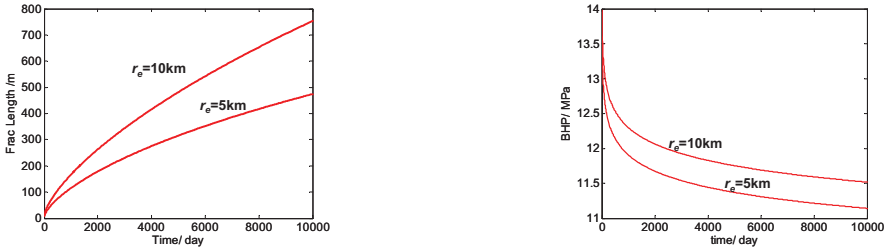

(a) (b)

Figure 16. The effect of formation drainage radius on bottom hole pressure in fracture propagation; (b) bottom hole pressures of formations with 5km and 10km drainage radius.

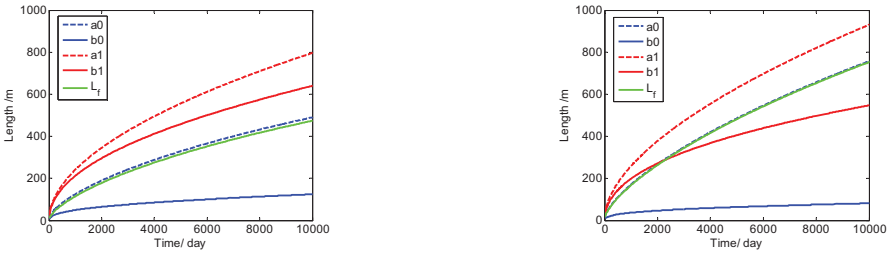

(a) (b)

Figure 17. The effect of formation drainage radius on fracture growth and injected CO_2 migration: (a) r_e=5km; (b) r_e=10km.

3.3. Comparisons of single-phase and two-phase flow model

Comparing two panels in Fig. 18, we find fracture grows faster with two-phase flow model (803 m) and CO_2 flooded region is more round with two-phase flow model (a_1/b_1 equals 1.36) than those of single-phase model with fracture length 753 m and a_1/b_1 equals 1.71 after 10000 days injection. In two-phase flow model, flood front moves faster to 1182 m in major direction after 10000 days injection compared to 931 m by single-phase flow model. It The fracture grows faster in two-phase flow model because it requires higher bottomhole pressures, shown in Fig. 19(a). Hence, injectivity is overestimated by single-phase model as shown in Fig. 19(b).

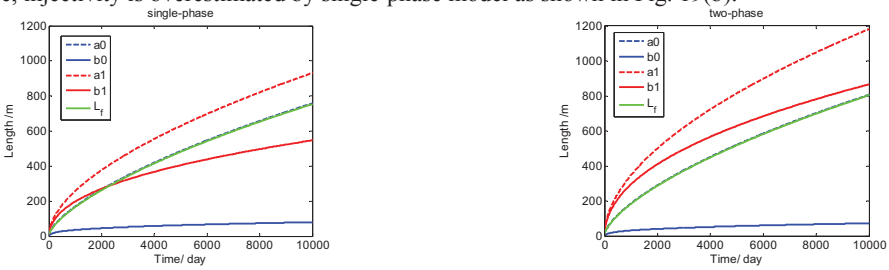

(a) (b)

Figure 18. Comparison of single-phase model with two-phase model on fracture growth and fronts growth with formation drainage radius,

r_e =10 km: (a) single phase; (b) two-phase.

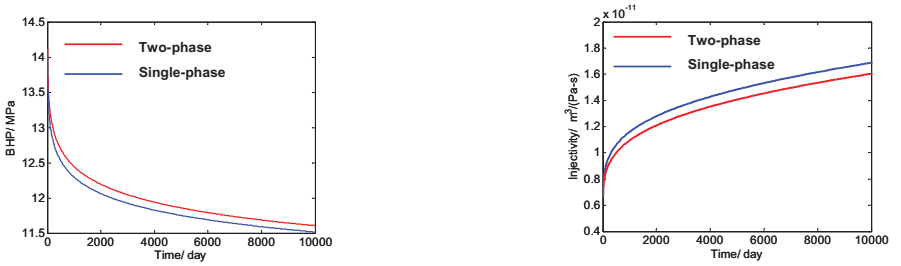

Figure 19. Comparison of single-phase model with two-phase model on (a) bottomhole pressure and (b) injectivity of the case in Fig. 18.

As we mentioned in the last part of model, volume of cooled region (V_T) may or may not be larger than pure CO_2 region (V_{dry}). By investigating porosity and volumetric rock heat capacity, we demonstrate both cases are possible to exist during CO_2 injection process. As the two cases in Fig. 20, in low porosity and high volumetric rock heat capacity formation, V_T is smaller than V_{dry}, and vice versa.

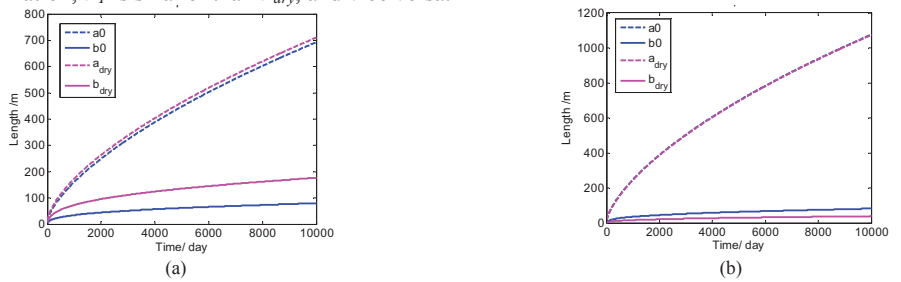

Figure 20. Two injection scenarios corresponds to the cases in Fig. 7: (a) $V_{dry}>V_T$ with ϕ =0.1, $\rho_{gr}C_{gr}$=2340 kJ/(m^3-K); (b) $V_{dry}<V_T$ with ϕ =0.3, $\rho_{gr}C_{gr}$=1170 kJ/(m^3-K). Blue curves and magenta curves stand for the major and minor axes of thermal front and dry front (interface of pure CO_2 zone and two-phase zone).

4. Conclusions

By extending Buckley-Leverett fractional flow theory in elliptical coordinate system, we successfully incorporated two-phase flow model to semi-analytical model of injection induced fracture. The improvement enables CO_2-brine mutually soluble mixture region in CO_2-brine migration system, which allows more accurately predict flow performance from fractured vertical injectors. This two-phase flow model corrects the underestimated bottomhole pressure by single phase model and yields longer fractures.

We also investigate fracture growth in various injection scenarios by parametric analysis and obtain the following conclusions:

(1) fracture growth speed directly determines shape of CO_2 flooded region and migration speed of flood front
(2) fracture length is non-linear to injection rate at low injection rate and linear to that at high injection rate
(3) fracture grows fast in formations with high Young's modulus and have a quick breakthrough and low usage efficiency of storage site; in formations with low Young's modulus, fracture grows slowly and may stop at short length, which results in a nearly circle flooded region and long breakthrough time with high storage site usage efficiency
(4) the influence of Poisson's ratio is not strong on injection induced fracture growth
(5) fracture grows very fast in over-pressured formation

(6) fracture grows fast in high porosity formation where storage site usage efficiency is low
(7) fracture grows fast in formation with low volumetric rock heat capacity
(8) the influence of formation thickness on fracture growth is higher than that of formation permeability even conductivity of two formations are the same
(9) fracture grows faster in high porosity formation where storage site usage efficiency is low
(10) small size storage site provides better storage site usage efficiency as flooding region is more round

Acknowledgements

We are grateful to the sponsors of Geologic CO_2 Storage Industrial Associates Project at The University of Texas at Austin: BP, Chevron, ExxonMobil, Statoil and the USGS.

References

[1] Luo Z, Bryant SL, Influence of thermo-elastic stress on fracture initiation during CO_2 injection and storage, GHGT-10, Amsterdam, Netherland, 2010
[2] Perkins TK, Gonzalez JA, The effect of thermoelastic stresses on injection well fracturing, Old SPE Journal, 25(1), 1985, 78-88.
[3] Luo Z, Modeling injection induced fractures and their impact in CO_2 geological storage, Ph.D dissertation, The University of Texas at Austin, 2013
[4] Hagoort J, Weatherill B, Settari A, Modeling the propagation of waterflood-induced hydraulic fractures, SPE Journal, 20(4), 1980, 293-303.
[5] Luo Z, Bryant SL, Influence of thermo-elastic stress on CO_2 injection induced fractures during storage, SPE 139719, International Conference on CO_2 Capture, Storage, and Utilization held in New Orleans, Louisiana, USA, 2010
[6] Noh M, Lake L, Bryant SL, Araque MA, Implications of coupling fractional flow and geochemistry for CO_2 injection in aquifers, SPE Reservoir Evaluation & Engineering, 10(4), 2007, 406-414
[7] Burton M, Kumar N, Bryant SL, Time-dependent injectivity during CO_2 storage in aquifers, International SPE/DOE Symposium on Improved Oil Recovery, Tulsa, Oklahoma, USA, 2008